Advances in Applied Mathematics and Mechanics
Adv. Appl. Math. Mech., Vol. **xxx**, No. x, pp. 1-25

DOI: 10.4208/aamm.OA-2021-0237
xxx 2023

# Application of 2-D GDQ Method to Analysis a Thick FG Rotating Disk with Arbitrarily Variable Thickness and Non-Uniform Boundary Conditions

Hodais Zharfi*

*Faculty of Engineering, Esfarayen University of Technology, Esfarayen, Iran*

Received 20 July 2021; Accepted (in revised version) 5 April 2022

**Abstract.** In this paper two-dimensional differential quadrature method has been used to analyze thick Functionally Graded (FG) rotating disks with non-uniform boundary conditions and variable thickness. Material properties vary continuously along both radial and axial directions by a power law pattern. Three-dimensional solid mechanics theory is employed to formulate the axisymmetric problem as a second order system of partial differential equations. The non-uniform boundary conditions are exerted directly into the governing equations to reach the eigenvalue system of equations. Four different disk profile shapes are considered and discussed. The effect of the power law exponent is also investigated and results show that by the use of material which functionally varied along the radial and especially axial directions the stresses and strains can be controlled so the capability of the disk is increased. Comparison with other available approaches in the literature shows a good agreement here in terms of computational time, robustness and accuracy of the present method. Moreover, novel applications are shown to provide results for further studies on the same topics.

**AMS subject classifications**: 74G15

**Key words**: Thick rotating disk, FG material, 2-D GDQ, variable thickness, profile shape, non-uniform boundary condition, 2-D material gradient.

## 1 Introduction

A most used structural element in many rotating machineries is rotating disks, they have many practical engineering applications such as turbo generators, casting ship propellers, turbojet engines, steam and gas turbine, reciprocating and centrifugal compressors, pumps and brake disk of automobiles. In all these applications, the total stresses due to centrifugal load have important effects on their strength and safety. Thus, control and optimization of total stresses and displacements field is an important designing

*Corresponding author.
*Email:* zharfi@esfarayen.ac.ir (H. Zharfi)

 

task [1]. Therefore more researches have been done on rotating disk analysis some of which are mentioned here. Afsar et al. [2] studied a thin circular FGM disk subjected to a thermo-elastic field using the finite element method. They reveal that the thermo-elastic field in FGM disks is significantly influenced by temperature distribution, the angular speed of the disk and the inner and the outer surface temperature difference. Asghari and Ghafoori [3] presented a two dimensional plate stress analysis for a three dimensional FGM rotating disk. Their results showed that although the plane-stress solution satisfies all the governing three dimensional equations of motion and boundary conditions it fails to give a compatible three dimensional strain field and it is not a valid solution. They modified the plane stress solution to reach an adequate three dimensional solution for a thick FGM rotating disk. Vullo et al. [4] presented an analytical procedure for the evaluation of elastic stresses and strains in a non-linear variable thickness rotating disk. They defined a density variation along the radial direction and a relation between the stress state and displacement field. They demonstrated that the results obtained by this method perfectly match those obtained by FEA. Nie et al. [5] analyzed the axisymmetric deformation of an isotropic rotating disk with its thickness, mass density, thermal expansion coefficient and shear modulus varying in the radial direction. They used the differential quadrature method for solving the non-homogeneous ordinary differential equations with variable coefficients for airy function. They also analyzed the challenging problem of tailoring the variation of either the shear modulus or the thermal expansion coefficient in the radial direction. Jahed et al. [6] considered an inhomogeneous disk model with variable thickness and used the variable material properties method to obtain the stress field under rotation and a steady temperature field. They modeled the rotating disk as a series rings of different but constant properties and arrived the optimum disk profile by sequentially proportioning the thickness of each ring to satisfy the stress requirements. Alexandrova et al. [7] studied the plane state of stress in an elastic-perfectly plastic isotropic rotating annular disk with constant thickness and density mounted on a rigid shaft. Hosseini et al. [8] present the stress analysis of a rotating nano-disk made of functionally graded materials with non-linearity varying thickness based on strain gradient theory. They examined the effects of various parameters such as graded index and thickness profile on stresses. Their results show that the effect of thickness parameters is greater than the effect of the graded index and the difference between the stress predicted by the classical theory and the strain gradient theory is large when the thickness of the nano-disk is small. Farshi et al. [9] considered an inhomogeneous disk with variable thickness and used the variable material properties and an optimization process to calculate the stress and optimized the disk profile.

Functionally graded materials (FGM) are composites in which the volume fraction, sizes and shapes of materials constituents can be varied continuously to get desired smooth spatial variations of macroscopic properties such as the elastic modulus, mass density, shear modulus, heat conductivity, etc. [3]. The functionally graded materials are the materials with the designing capability and are usually confirmed from metals and ceramics phase. Based on an adequate mixture rule, the volume fraction of each phases

prescribed the composition properties in each point of composite material. It means the functionally graded materials are characterized by gradually changed physical properties [10].

To solve an engineering problem, the condition around the boundary of the area under consideration must be specified certainly. It is obvious that the boundary conditions effects seriously the governing equations and response functions. Uniform boundary conditions which are used in many articles exist in the literature, lead to an uniform eigenvalue system of equations therefore a simpler solution. The non-uniformity in the boundary conditions may take either the discontinuous type (usually referred to as mixed boundary conditions) or the continuous non-uniform type (that is varying elastically restrained conditions) [11]. Furthermore, there are many useful numerical methods for solving the equations describing the engineering problems, which their closed form solution are difficult to establish. Finite elements, finite difference, differential quadrature, and boundary element methods are among the numerical solution methods [12]. Considerable research has been done on stress and strain analysis in rotating disks with various boundary conditions using various techniques such as the nonlinear graded finite element method [13], finite difference method [14], variable material properties (VMP) method [15, 16], meshless method based on the local Petrov-Galerkin approach [17], homotopy analysis method [18] and generalized differential quadrature method [19]. The generalized differential quadrature method is utilized for solving a variety of problems because of its high accuracy, reliability and general applicability. In this numerical method, the function derivatives are approximated in terms of linear summation of the production of function value and weighting coefficients in various grid points [20]. At first Bellman et al. [21] proposed the differential quadrature method and suggested two techniques for the first order weighting determination. Shu et al. [22] developed a generalized differential quadrature method to overcome the restrictions existing in Bellman's method. Differential quadrature and the generalized differential quadrature methods have been used to solve many different engineering problems such as: bending analysis of thin isotropic circular plates [23], vibration analysis of arbitrarily shaped laminated composite shells [24], static analysis of laminated composite rectangular and annular plates with a posteriori shear and normal stress recovery [25], non-steady creep analysis of FGM rotating thin disk [26], nonlinear bending analysis of a single SWCNT over a bundle of nanotubes [27], static and free vibration analysis of free-form laminated Doubly-Curved shells and panels of revolution resting on Winkler-Pasternak elastic foundations [28]. The incorporation of boundary conditions and the selection of grid point distribution are two main complicated and effective problems in GDQ implementation. Laura and Gutierrez [29] used a $\delta$-technique for using the GDQ method in the vibration analysis of rectangular plates having non-uniform boundary conditions. This technique was proposed by Bert et al. [30] and Jang et al. [31]. In this technique, a series of two grid points are separated from each other by a small distance $\delta$ near the boundary edges. Since the $\delta$ parameter must be selected very small, the DQ weighting coefficients matric may become ill-conditioned thereby creating undesirable oscillations of solution [11].

Shu et al. [32] presented a new methodology for implementing the clamped and simply supported boundary conditions for the free vibration analysis of beams and plates using the generalized differential quadrature method. They proposed this approach to overcome the drawback of the previous approach in treating the boundary conditions and compared this method with the other adjustment solution method such as the method of modifying weighting coefficient matrices.

The literature review shows that the majority of the carried out research is concentrated on thin functionally graded rotating disks with thin constant thickness and using the plane stress assumption. It is obvious the plane stress assumption can not be applied to thick disks not at all. In most research exist in the literature the material properties are assumed to vary only in one direction whiles mostly conventional functionally graded materials might not be that effective in such design problems. Using the one dimensional pattern of heterogeneity might not be an accurate model for thick disk analysis and cause a noticeable errors. Furthermore using two dimensional pattern of functionally graded materials leads to an exact and flexible design of materials that provides accurate results [33, 34]. Furthermore, all applications of the GDQ method in the literature are restricted to the uniform geometrical model, this restriction is not satisfactory. In this paper the two dimensional generalized differential quadrature method is used to solve the governing equation of an FGM rotating thick disk with variable thickness. For this purpose, the two dimensional governing equations of FGM rotating thick disk with variable thickness and variation of particle reinforcement along both radial and axial directions are derived and solved using the 2-D GDQ method for non-uniform boundary conditions.

Near the most existing analyses with generalized differential quadrature methods in the literature are confined to a uniform geometrical model, this restriction is obviated in this paper. Despite all existing complexities such as the application of non-uniform boundary conditions and non-uniform geometrical models, variation of material properties along both radial and axial directions and the system of nonlinear equations, the convergence of the final response is very fast. This model obviates many of the simplifications and restrictions which are associated with other solution methods in FGM rotating disk analysis.

## 2 Mathematical formulation

Let a two dimensional FG rotating thick disk with inner radius a and outer radius $b$ with variable thickness $h(r)$ depicted in Fig. 1(a). The present study considers the disk in axisymmetric conditions so that only the generic radius is investigated as a two-dimensional domain (all the contributions about $\theta$ are neglected as well as $u_\theta$ and all the derivatives with respect to $\theta$ direction). The disk is fixed at the inner radius and the outer surface of the disk is traction free so the boundary conditions of the problem are non-uniform. Such

boundary conditions can be written as:

$$\begin{cases} r=a: & u(r,z)=0, \quad w(r,z)=0, \\ r=b: & \sigma_r(r,z)=0, \quad \tau_{rz}(r,z)=0, \end{cases} \quad \begin{cases} z=-h/2: & \sigma_z(r,z)=0, \quad \tau_{rz}(r,z)=0, \\ z=h/2: & \sigma_z(r,z)=0, \quad \tau_{rz}(r,z)=0. \end{cases} \tag{2.1}$$

By considering the generic element of rotating disk in Fig. 1(b), the equilibrium equations are derived as

$$\begin{cases} \dfrac{\partial \sigma_r}{\partial r}+\dfrac{\sigma_r-\sigma_\theta}{r}+\dfrac{\partial \tau_{rz}}{\partial z}+\rho r\omega^2=0, \\ \dfrac{\partial \tau_{zr}}{\partial r}+\dfrac{\partial \sigma_z}{\partial z}+\dfrac{\tau_{zr}}{r}=0. \end{cases} \tag{2.2}$$

Where, $\sigma_r$, $\sigma_\theta$, $\sigma_z$ and $\tau_{rz}$ are the radial, circumferential, axial and shear stresses, respectively. $\rho$ is the material density and $\omega$ is the rotating speed. Using stress-strain and strain-displacement relations, it is concluded that:

$$\begin{cases} \varepsilon_r=\dfrac{\partial u}{\partial r}=\dfrac{1}{E}[\sigma_r-v(\sigma_\theta+\sigma_z)], \\ \varepsilon_\theta=\dfrac{u}{r}=\dfrac{1}{E}[\sigma_\theta-v(\sigma_r+\sigma_z)], \\ \varepsilon_z=\dfrac{\partial w}{\partial z}=\dfrac{1}{E}[\sigma_z-v(\sigma_r+\sigma_\theta)], \\ \varepsilon_{rz}=\dfrac{1}{2}\left(\dfrac{\partial w}{\partial r}+\dfrac{\partial u}{\partial z}\right)=\dfrac{\tau_{rz}}{G}. \end{cases} \tag{2.3}$$

In the above relations, $\varepsilon_r$, $\varepsilon_\theta$, $\varepsilon_z$ and $\varepsilon_{rz}$ are the radial, tangential, axial and shear strain components, respectively. $u$ and $w$ are the radial and axial displacements. $E$ and $G$ are the elasticity and shear modulus respectively and $\nu$ is the Poisson ratio. From the above set of equations, the stress-displacement relations can be extracted as Eq. (2.4)

$$\begin{cases} \sigma_r=\dfrac{E(1-v)}{1-v-2v^2}\dfrac{\partial u}{\partial r}+\dfrac{Ev}{1-v-2v^2}\dfrac{u}{r}+\dfrac{Ev}{1-v-2v^2}\dfrac{\partial w}{\partial z}, \\ \sigma_\theta=\dfrac{Ev}{1-v-2v^2}\dfrac{\partial u}{\partial r}+\dfrac{E(1-v)}{1-v-2v^2}\dfrac{u}{r}+\dfrac{Ev}{1-v-2v^2}\dfrac{\partial w}{\partial z}, \\ \sigma_z=\dfrac{Ev}{1-v-2v^2}\dfrac{\partial u}{\partial r}+\dfrac{Ev}{1-v-2v^2}\dfrac{u}{r}+\dfrac{E(1-v)}{1-v-2v^2}\dfrac{\partial w}{\partial z}, \\ \tau_{rz}=G\left(\dfrac{\partial w}{\partial r}+\dfrac{\partial u}{\partial z}\right). \end{cases} \tag{2.4}$$

After substituting stresses from Eq. (2.4) into governing equilibrium equations the Navier form governing equations are established as below:

$$\begin{cases} \lambda_1\dfrac{\partial^2 u}{\partial r^2}+\lambda_2 d\dfrac{\partial^2 u}{\partial z^2}+\lambda_3\dfrac{\partial^2 w}{\partial r\partial z}+\lambda_4\dfrac{\partial u}{\partial r}+\lambda_5\dfrac{\partial u}{\partial z}+\lambda_6\dfrac{\partial w}{\partial r}+\lambda_7\dfrac{u}{r}+\rho r\omega^2=0, \\ \beta_1\dfrac{\partial^2 w}{\partial z^2}+\beta_2\dfrac{\partial^2 u}{\partial r^2}+\beta_3\dfrac{\partial^2 u}{\partial r\partial z}+\beta_4\dfrac{\partial u}{\partial r}+\beta_5\dfrac{\partial u}{\partial z}+\beta_6\dfrac{u}{r}+\beta_7\dfrac{\partial w}{\partial r}+\beta_8\dfrac{\partial w}{\partial z}=0. \end{cases} \tag{2.5}$$

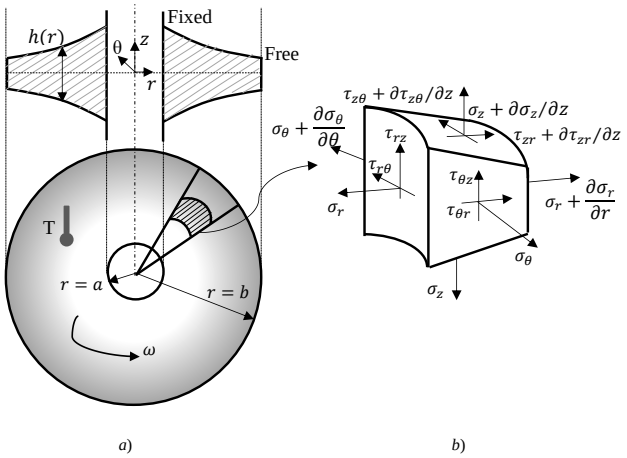


Figure 1: Disk specification and element conditions.

Where $\lambda_1-\lambda_7$ and $\beta_1-\beta_8$ are coefficients that depend on material properties which vary along both radial and axial directions. Definitions of such coefficients are given in the appendix.

As it was aforementioned, all mechanical and thermal properties of FG rotating thick disks are a function of the radial and transverse directions of the disk. Material properties will be introduced in the next section.

## 3 Volume fraction and material distribution

In recent years the fabrication and processing method of Functionally Graded (FG) materials has been developed significantly. Using the computer-aided manufacturing process it is possible to produce functionally graded materials with two or three dimensional gradients. The inner surface of a rotating disk usually experiences a larger amount of stress so it is necessary to reinforce this part by using high-strength materials. For this reason in this paper the inner surface is considered to be made of two different metals. Furthermore, for obviating the temperature resistance property, the outer surface of the disk is made of two different ceramics. The volume fraction of the materials is varied continuously as a function of both radial and transverse directions as indicated below:

$$\begin{cases} v_{m_1}(r,z)=\left[1-\left(\dfrac{r-a}{b-a}\right)^{n_r}\right]\left[1-\left(\dfrac{z+h(r)}{2h(r)}\right)^{n_z}\right], \\ v_{m_2}(r,z)=\left[1-\left(\dfrac{r-a}{b-a}\right)^{n_r}\right]\left[\dfrac{z+h(r)}{2h(r)}\right]^{n_z}, \\ v_{C1}(r,z)=\left[\dfrac{r-a}{b-a}\right]^{n_r}\left[1-\left(\dfrac{z+h(r)}{2h(r)}\right)^{n_z}\right], \\ v_{C2}(r,z)=\left[\dfrac{r-a}{b-a}\right]^{n_r}\left[\dfrac{z+h(r)}{2h(r)}\right]^{n_z}, \end{cases} \tag{3.1}$$

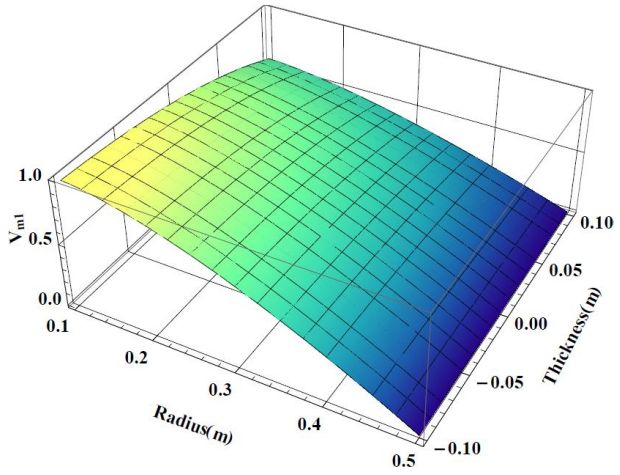


Figure 2: Volume fraction of first metal.

where $m_1$, $m_2$, $c_1$ and $c_2$ refer to the first metal, second metal, first ceramic and second ceramic respectively. $a$ and $b$ are the inner and outer radii of the disk which are selected to be 0.1m and 0.5m respectively. $h(r)$ is the variable thickness, $n_r$ and $n_z$ are the volume fraction exponents along the $r$ and $z$ directions. By using a linear mixture rule the material properties at each point can be obtained. For instance if $\Psi$ defines a generic material property, it can be determined by a linear combination of volume fractions and the same properties of each constituent

$$\psi = \psi_{c1} v_{c1} + \psi_{c2} v_{c2} + \psi_{m1} v_{m1} + \psi_{m2} v_{m2}. \tag{3.2}$$

Values of $n_r$ and $n_z$ change the distribution pattern, for example if $n_z = 0$ or $n_r = 0$ the volume fraction reduces to a one-dimensional functionally graded distribution. The volume fraction distribution for the first metal by selecting $n_r = 1.5$ and $n_z = 3$ for constant thickness is presented in Fig. 2.

## 4 Solution method

The governing equation of FG rotating thick disks has been derived in section 2 and material properties have been defined in Section 3. Due to the complexity of the differential problem at hand a numerical method to solve the given system of equations must be used. As it was aforementioned, the 2-D generalized differential quadrature method is used for solving the present problem. In this solution method the partial differential of a function with respect to a coordinate direction is expressed as a linear weighted sum of all functional values at all grid points in that direction [19].

For a smooth function $f(r,z)$, 2-D GDQ discretized its $n$th and $m$th order derivatives

with respect to $r$ and $z$ at the grid point $(r_{ij},z_{ij})$ on the non-uniform area as:

$$f_r^{(n)}\left(r_{ij},z_{ij}\right)=\frac{\partial^n f(r,z)}{\partial r^n}\bigg|_{z=z_{ij}}^{r=r_{ij}}=\sum_{k=1}^{N}a_{ik}^{(n)}f\left(r_{kj},z_{kj}\right),\quad i=1,2,\cdots,N,\quad n=1,2,\cdots,N-1, \tag{4.1a}$$

$$f_z^{m}\left(r_{ij},z_{ij}\right)=\frac{\partial^m f(r,z)}{\partial z^m}\bigg|_{z=z_{ij}}^{r=r_{ij}}=\sum_{l=1}^{M}b_{jl}^{(m)}f\left(r_{jl},z_{il}\right),\quad j=1,2,\cdots,M,\quad m=1,2,\cdots,M-1, \tag{4.1b}$$

$$f_{rz}^{(n+m)}\left(r_{ij},z_{ij}\right)=\frac{\partial^{(n+m)} f(r,z)}{\partial r^n\partial z^m}\bigg|_{z=z_{ij}}^{r=r_{ij}}=\sum_{k=1}^{N}a_{ik}^{(n)}\sum_{l=1}^{M}b_{jl}^{(m)}f(r_{kl},z_{kl}),\quad i=1,2,\cdots,N,$$
$$j=1,2,\cdots,M,\quad n=1,2,\cdots,N-1,\quad m=1,2,\cdots,M-1, \tag{4.1c}$$

where $N$ and $M$ are the number of grid points in the $r$ and $z$ directions respectively. $a_{ik}^{(n)}$ and $b_{jl}^{(m)}$ are the weighting coefficients of order $(n)$ and $(m)$ along the $r$ and $z$ direction respectively. These coefficients can be defined on the non-uniform area using the first order derivatives as below:

$$a_{ij}^{(n)}=\begin{cases} na_{ii}^{(n-1)}a_{ij}^{(1)}-\frac{a_{ij}^{(n-1)}}{r_{ij}-r_{jj}}, & j\neq i,\\ \sum\limits_{k=1,k\neq i}^{N}a_{ik}^{(n)}, & j=i,\end{cases}\qquad i,j=1,2,\ldots,N,\quad n=2,3,\ldots,N-1, \tag{4.2a}$$

$$b_{ij}^{(m)}=\begin{cases} mb_{ii}^{(m-1)}b_{ij}^{(1)}-\dfrac{b_{ij}^{(m-1)}}{z_{ii}-z_{ij}}, & i\neq j,\\ \sum\limits_{l=1,l\neq i}^{M}b_{il}^{(m)}, & i=j,\end{cases}\qquad i,j=1,2,\ldots,M,\quad m=2,3,\ldots,M-1. \tag{4.2b}$$

In the above equations $a_{ij}^{(1)}$ and $b_{ij}^{(1)}$ are the first weighting coefficients which are given by:

$$a_{ij}^{(1)}=\begin{cases} \dfrac{A^{(1)}\left(r_{ij}\right)}{\left(r_{ij}-r_{jj}\right)A^{(1)}\left(r_{jj}\right)}, & i\neq j,\\ -\sum\limits_{k=1,k\neq i}^{N}a_{ik}^{(1)}, & i=j,\end{cases}\qquad i,j=1,2,\ldots,N, \tag{4.3a}$$

$$b_{ij}^{(1)}=\begin{cases} \dfrac{B^{(1)}\left(z_{ii}\right)}{\left(z_{ii}-z_{ij}\right)B^{(1)}\left(z_{ij}\right)}, & i\neq j,\\ -\sum\limits_{l=1,l\neq i}^{M}b_{il}^{(1)}, & i=j,\end{cases}\qquad i,j=1,2,\ldots,M. \tag{4.3b}$$

Where,

$$A^{(1)}(r_{ij}) = \prod_{k=1,k\neq i}^{N} (r_{ij} - r_{kj}), \tag{4.4a}$$

$$B^{(1)}(z_{ij}) = \prod_{k=1,k\neq j}^{M} (z_{ij} - z_{ik}). \tag{4.4b}$$

For calculating the weighting coefficients, the coordinates of grid points must be known, various grid points distributions are studied in the literature, in this study the roots of Chebyshev polynomial of the first kind used for grid point generation in radial and transverse directions as:

$$r_{ij} = a + 0.5\left[1 - \cos\left(\frac{i-1}{N-1}\pi\right)\right](b-a), \tag{4.5a}$$

$$z_{ij} = -\frac{h_i}{2} + 0.5\left[1 - \cos\left(\frac{j-1}{M-1}\pi\right)\right]h_i. \tag{4.5b}$$

In Eq. (4.5b), $h_i$ is the thickness of the disk in $r_{ij}$. Two dimensional generalized differential quadrature method represented by the above formulations was applied to analyze the thick FG non-constant thickness disk and showed high capacity in accurate, fast and efficient computational operations.

## 5 Numerical application and discussion

Before providing the results of a thick disk the solution algorithm must be validated. For this purpose, the present results for FG rotating disks are compared to a finite element solution [33]. For the present comparison the inner radius $a = 0.2$ and outer radius $b = 0.5$ and a linear profile shape is considered. The material constituents are selected to be same and for $n_r = 2$ and $n_z = 1.5$ results are achieved and for instance the radial displacement comparison is presented in Fig. 3. As it can be seen, it shows a good agreement between the results.

In the following, a thick rotating disk made of 2-D FG material and a non-uniform profile is considered. The disk has non-uniform boundary conditions; claimed at the inner radius and free at other boundary surfaces. The rotational speed of the disk is considered to be 500rad/s. The thickness of the disk is varied along the radial direction in the form of Eq. (5.1)

$$h(r) = h_0\left(1 - q\left(\frac{r-a}{b-a}\right)^m\right), \tag{5.1}$$

where, $h_0$ is considered to be $0.5(b-a)$, $a$ and $b$ as explained earlier are the inner and outer radius respectively. As it can be seen for $m = 0$ the constant thickness is concluded and the combination of the values of $q$ and $m$ results in different thickness profile variations.

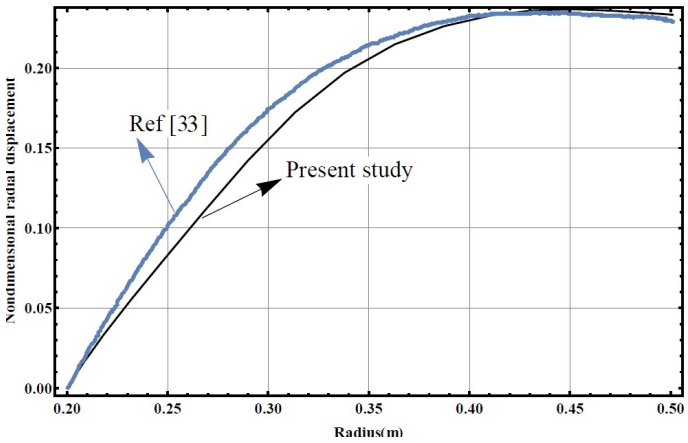


Figure 3: Non-dimensional radial displacement in radial direction compared with [33].

In this paper constant, linear, concave and convex profile shapes are considered. For different types of profile shapes the values of $q$ and $m$ are considered in Table 1.

Grid distribution as a function of the profiles indicated in Table 1 is depicted in Fig. 4. The volume fraction distribution is followed from Eq. (3.1). First metal used as $m_1$ is Titanium, the second metal is considered to be Aluminum, the first ceramic which named as $c_1$ is Silicon Carbide and second ceramic is supposed to be Alumina. Material properties at each point are obtained by using the properties of these materials in Table 2 and a suitable mixture rule as Eq. (3.2).

By using the above material properties in distinct profile shapes of thick disks the results of disk analysis are provided some of which are presented in this paper.

Radial, tangential, axial and equivalent stress distribution along the radial direction in constant profile shape for $n_r=2$, $n_z=3$ and at $z=0$, are presented in Fig. 5.

As can be seen the radial stress has a reduction trend along the radial direction, while the tangential and axial stresses almost increase through the radial direction. The equiv-

Table 1: Parameters of various profile shapes.

| Constant | Linear | Concave | Convex |
|---|---|---|---|
| $m=0, q=0$ | $m=1, q=0.7$ | $m=0.7, q=0.7$ | $m=2, q=0.7$ |

Table 2: Constituent material properties.

| | Titanium | Aluminum | Silicon Carbide | Alumina |
|---|---|---|---|---|
| $E$(GPa) | 100 | 70 | 450 | 390 |
| $G$(GPa) | 39 | 28 | 190 | 125 |
| $\rho$(Mg/m$^3$) | 4.5 | 2.7 | 3.2 | 3.4 |
| $\nu$ | 0.36 | 0.34 | 0.15 | 0.26 |

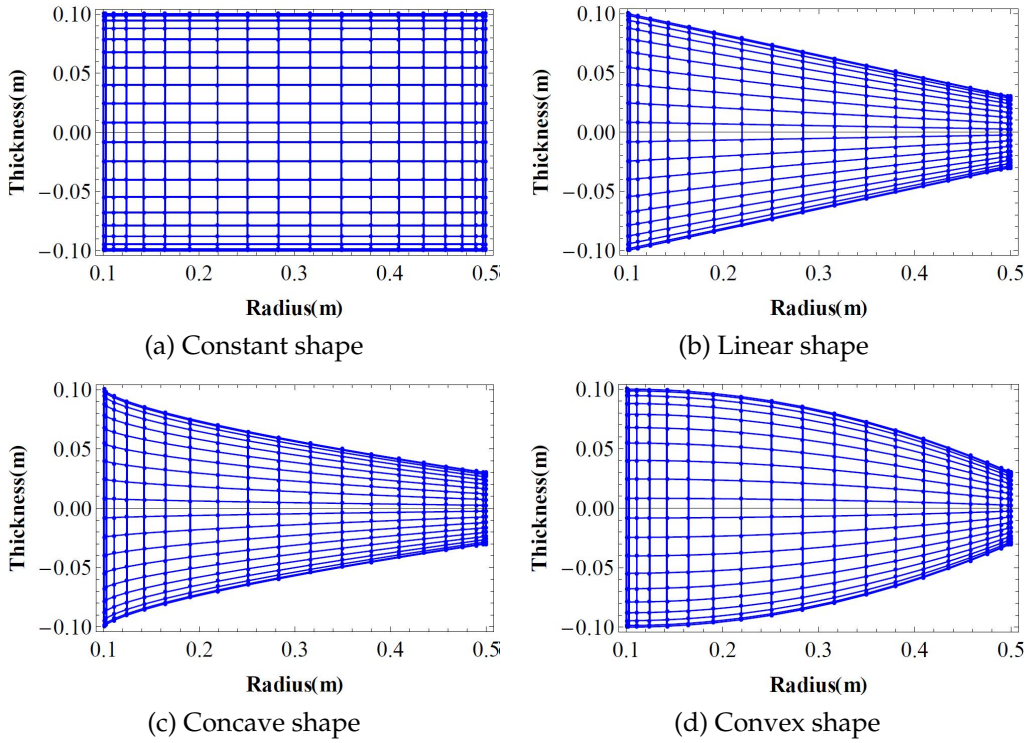


(a) Constant shape (b) Linear shape

(c) Concave shape (d) Convex shape

Figure 4: Four different profile shapes and grid point distribution.

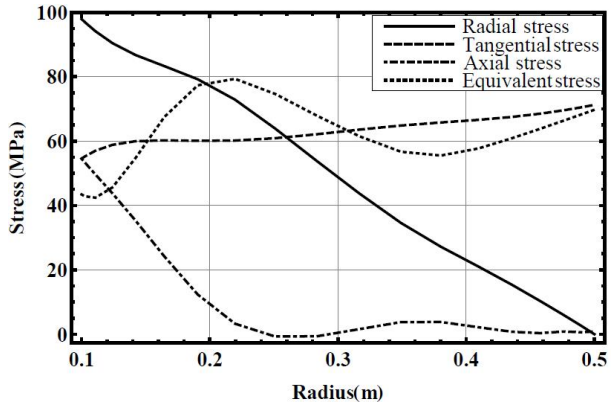


Figure 5: Stress distribution via radial direction at $z=0$ in constant profile shape with $n_r=2$, $n_z=3$.

alent stress reduced gradually along the radial direction and the maximum stresses occurred at the inner radius therefore it is necessary to reinforce the disk against the stresses at the inner radiuses.

Non-dimensional radial and axial displacement variation along the radial direction

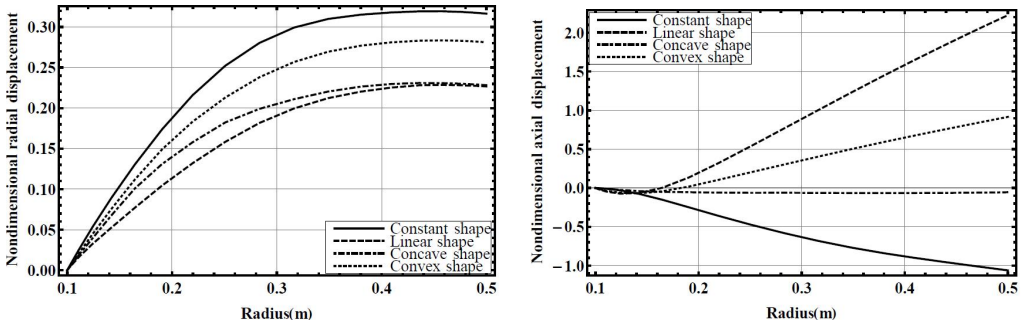


Figure 6: (a) Non-dimensional radial displacement and (b) Non-dimensional axial displacement distribution along the radial direction at $z=0$ with $n_r=1.5$, $n_z=3$ and for different profile shapes.

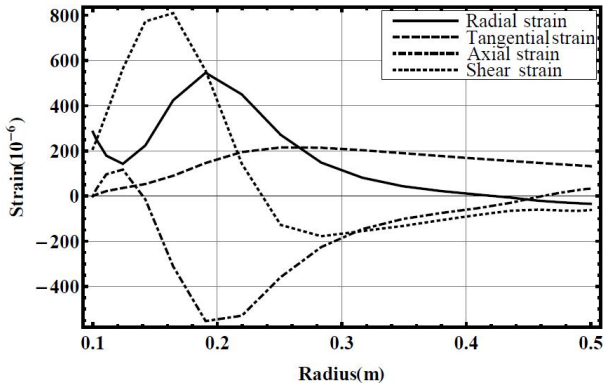


Figure 7: Strain distribution along the radial direction at $z=0$ in concave profile shape with $n_r=2$, $n_z=3$.

for $n_r=1.5$, $n_z=3$ and at the middle thickness of four different thickness profiles are shown in Fig. 6.

The non-dimensional radial displacement for all profile shapes rises along the radial direction and this rising for the constant profile shape is senior. Results show that the disk with linear and concave profile shapes has a better response. In the non-dimensional axial displacement as Fig. 6(b) shows in all profile shapes the rising trend is governed but it is obvious that this rising in constant and linear shape is serious. Disk with the concave profile shape has the lower axial displacement along the radial direction so it can be totally said that the disk with a concave profile shape has a better response in case of displacement distribution in the radial direction.

Fig. 7 shows the radial, tangential and axial strain distribution along the radial direction at $z=0$ for the concave type of thickness shape and $n_r=2$, $n_z=3$. The increasing-decreasing type of distribution for radial, tangential and shear strains is dominant, almost the highest value of strains occurred near the inner radius.

Fig. 8 illustrated the variation of radial, tangential, axial and shear strains along the

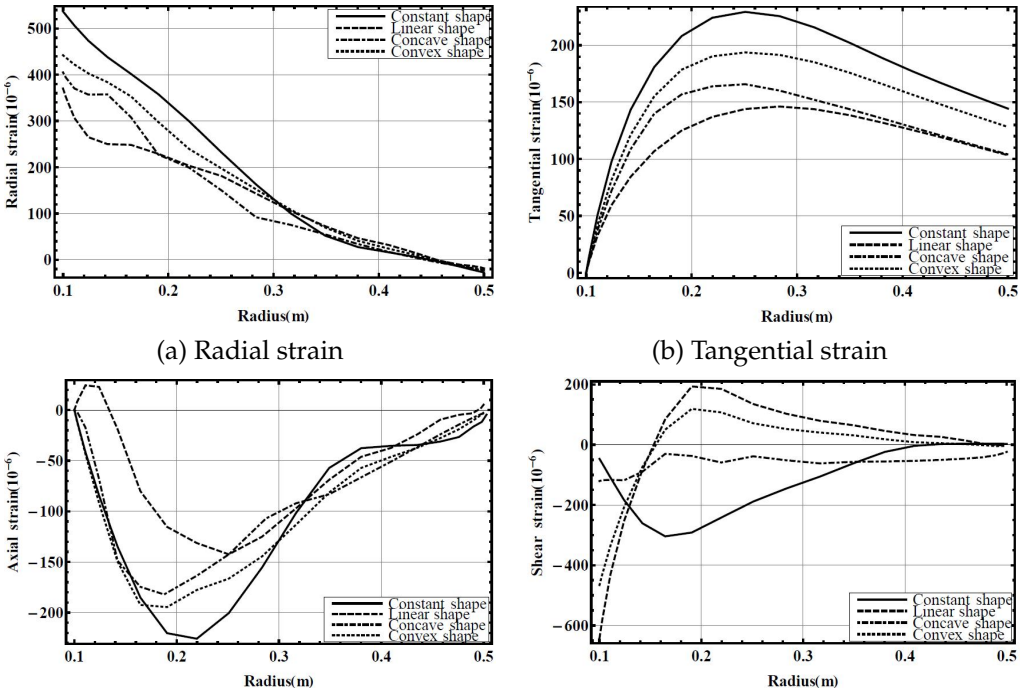


(a) Radial strain (b) Tangential strain

(c) Axial strain (d) Shear strain

Figure 8: Strain distribution along the radial direction at $z=0$ in various profile shapes with $n_r=1.5$, $n_z=3$.

radial direction at middle thickness for four different thickness profiles, respectively. As can be seen the constant profile shape has also the largest amount of strains too. So the constant profile shape is not appropriate.

Fig. 9 shows the variation of radial, tangential, axial and shear stresses along the radial direction at $z=0$ for different profile shapes, respectively. Radial and axial stresses decreased along the radius and almost tangential and shear stresses increased via the radial direction. This is evident that the constant profile shape has the largest value and the concave or linear profile shape has the lowest amounts of stresses.

Radial, tangential, axial and equivalent stresses distribution for a disk with convex profile shape and $n_r=2$, $n_z=3$ are presented in Fig. 10. For this profile shape the equivalent stress changes gently along the radius while the radial and axial stresses have relatively large changes along the radius.

Fig. 11 shows the non-dimensional radial and axial displacement variation in constant profile disk through the thickness of disk at four different radius distances with consideration of the material distribution power of $n_r=2$, $n_z=3$.

Radial and axial displacement increases along the thickness and whatever the distance from the inner radius increased this rising is larger. It means that the maximum value of displacement happened near the outer radiuses and upper surfaces. Because of

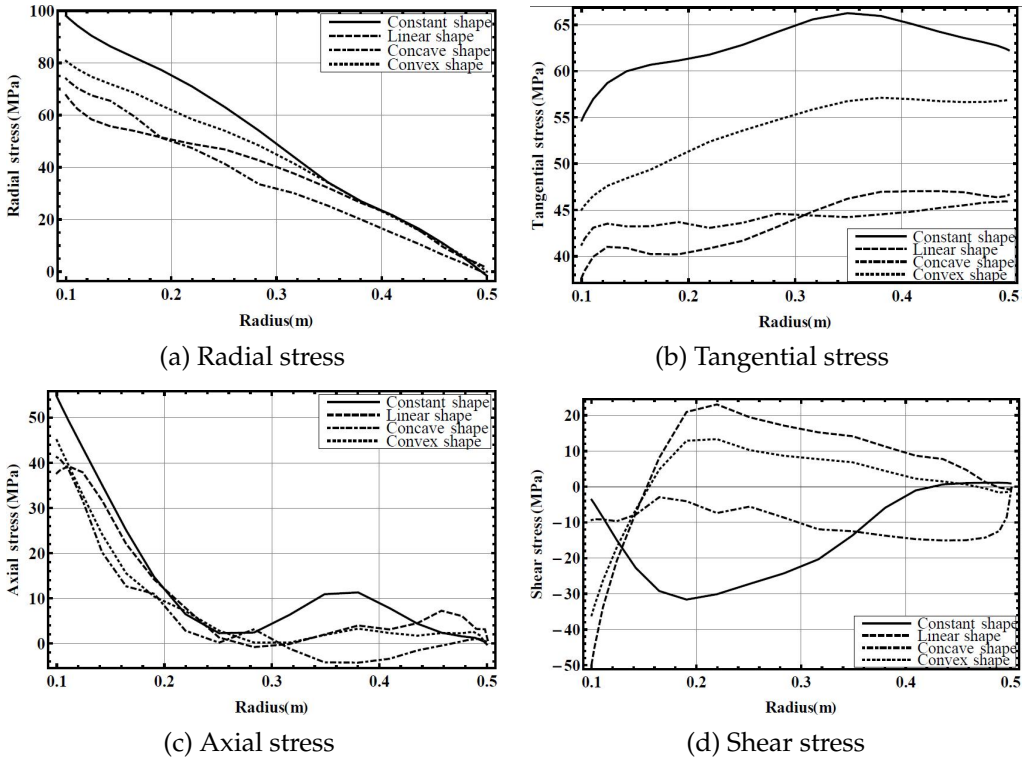


(a) Radial stress (b) Tangential stress

(c) Axial stress (d) Shear stress

Figure 9: Stress distribution along the radial direction at $z=0$ in various profile shapes with $n_r=1.5$, $n_z=3$.

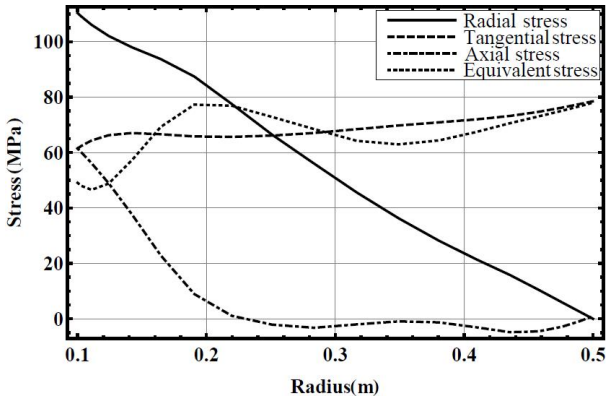


Figure 10: Stress distribution along the radial direction at $z=0$ for convex profile shape and $n_r=2$, $n_z=3$.

the power exponent of material properties along the thickness is non zero so the distribution of non-dimensional displacements is not symmetric with respect to $z=0$.

Similar to the previous figure, the non-dimensional axial and radial displacement distribution in convex profile disk with $n_r=2$, $n_z=3$ along the thickness direction at four

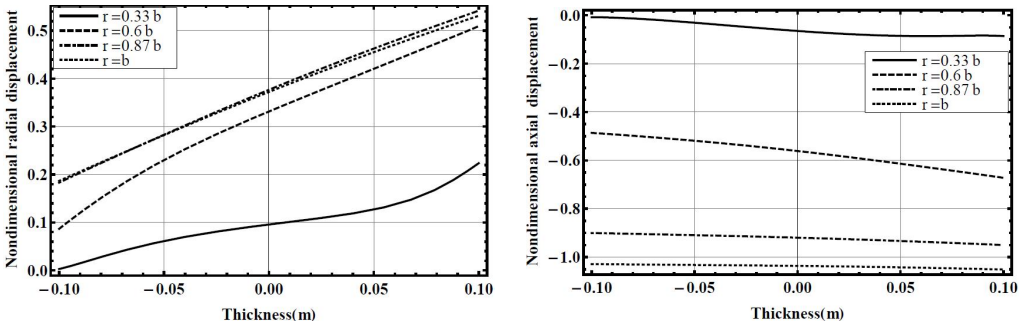


(a) Radial displacement (b) Axial displacement

Figure 11: Non-dimensional radial and axial displacement distribution via axial direction at four different radius.

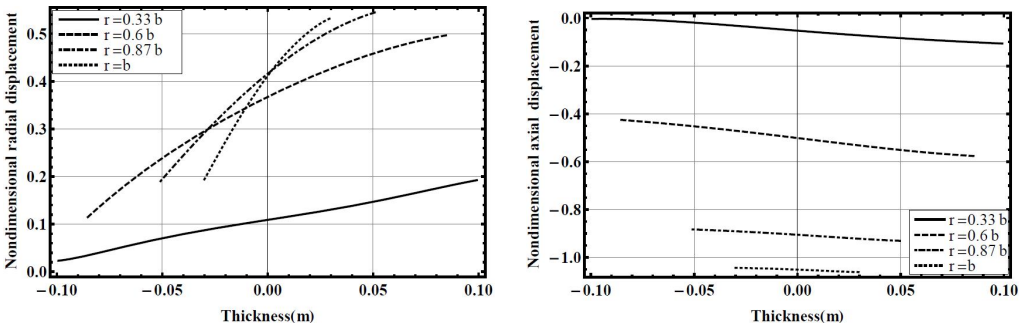


(a) (b)

Figure 12: Non-dimensional axial and radial displacement distribution via axial direction at four different radius.

different radius positions are also presented in Fig. 12.

This figure is also illustrated that displacements in the outer radius and upper thickness have larger amounts.

Fig. 13 presents the radial, tangential and axial strain along the thickness direction at $r = 0.33b$ for different types of thickness profiles. Results indicated that the distribution of strains along the thickness direction is depended on the profile shape of the disk entirely. So that the constant profile shape has a critical condition in comparison to the other profile shapes. Against the constant shape, the concave profile shape has better strain behavior along the axial direction. Since the boundary conditions of the disk at the upper and lower surface are free the shear strain at this location becomes zero.

For a better review and comparison, the 3-D distribution of radial strain, tangential strain, axial strain and shear strain for convex, constant, linear and concave profiles respectively with $n_r = 2$, $n_z = 3$ shown in Fig. 14.

Figures show that the strain distribution varied strongly along both radial and axial directions and plane stress assumption in thick disk situations leads to unacceptable results. As before, maximum variation pertaining to the inner radiuses and upper thick-

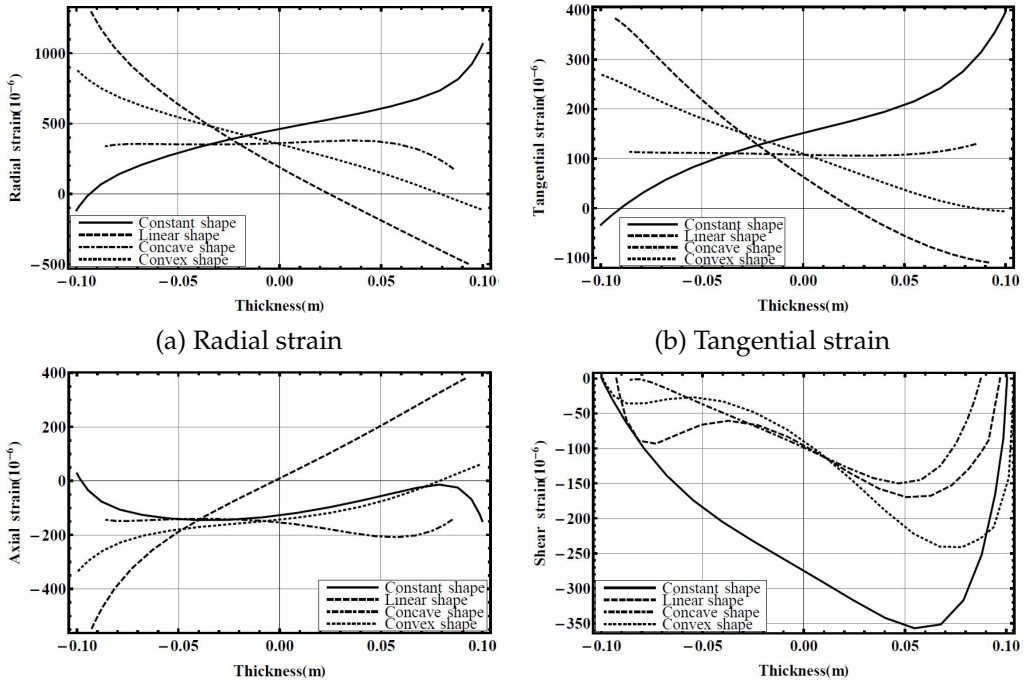


(a) Radial strain (b) Tangential strain

(c) Axial strain (d) Shear strain

Figure 13: Strain distribution via axial direction at $r=0.33b$ in four different profile shapes with $n_r=1.5$, $n_z=3$.

nesses. Therefore, the disk should be strengthened in the vicinity of its clamped position.

3-D distribution of radial, tangential, axial and shear stress for concave, convex, linear and constant profiles with $n_r=2$, $n_z=3$, respectively shown in Fig. 15. Radial and axial stresses vanish in the outer surface because of the free boundary condition at this surface. Radial, tangential and axial stresses experienced their larger amounts near the inner radius and upper thicknesses so the material strength at these points must be adequate.

Non-dimensional radial and axial displacements variations at the middle thickness and middle radius respectively, for the disk with linear thickness variation along the radius directions and power low exponent as $n_r=2$, $n_z=3$ are available in Fig. 16. Non-dimensional radial and axial displacements have the increasing trend along both radial and axial directions.

Non-dimensional stresses distributions along the radial and axial directions at various profile shapes with power exponent as $n_r=1.5$, $n_z=3$ proposed in Fig. 17. Results indicate that the biggest stresses occur at constant profile shape so the variable thickness shape is an essential choice in the field of disk design. By using the variable thickness, the stresses decrease and the disk's capacity to experience a bigger rotational speed is concluded. The effect of thickness shape on tangential stress and stress distribution along the axial direction is more appreciable.

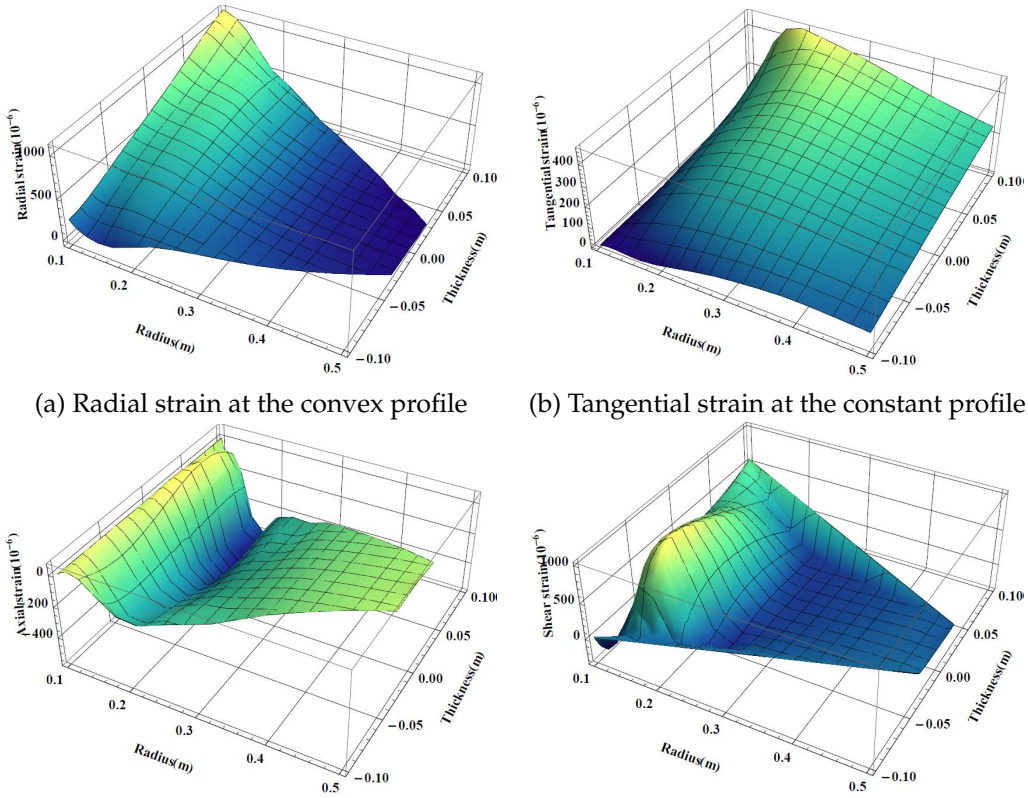


(a) Radial strain at the convex profile

(b) Tangential strain at the constant profile

(c) Axial strain at the linear profile

(d) Shear strain at the concave profile

Figure 14: 3-D Strain distribution with $n_r = 2$, $n_z = 3$.

Another influential factor in disk analysis is the material power exponents in radial and axial directions. For a more detailed analysis and assessment of the effect of material distribution power, four different combinations of power exponent is considered and the stress and strain distribution in this situation are extracted. Fig. 18 presents the Strain distribution in constant profile shapes with different combinations of material power exponents.

The results show that increasing the amount of radial distribution power $(n_r)$ will increase the strain values and increasing the amount of power distribution along the thickness $(n_z)$ reduces strain values. Therefore it can be said that the best composition of power exponent consists of the lower value of $n_r$ and the larger value of $n_z$. Fig. 19 illustrates the non-dimensional stress distribution along radial and axial directions for four different combinations of power exponents. Plot (a) in Fig. 19 shows that the distribution of radial stress along the radial direction does not change considerably with the power law exponents but the disk with $n_r = n_z = 0$ (isotropic disk) has higher radial stress in comparison with the functionally graded disk. Tangential stress is depended entirely on

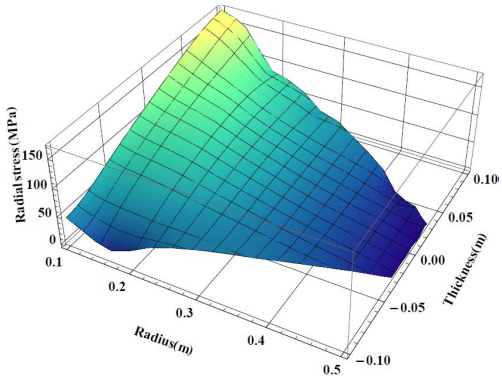


(a) Radial stress at the concave shape

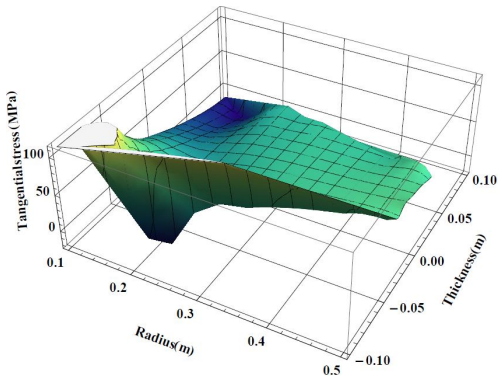


(b) Tangential stress at the convex shape

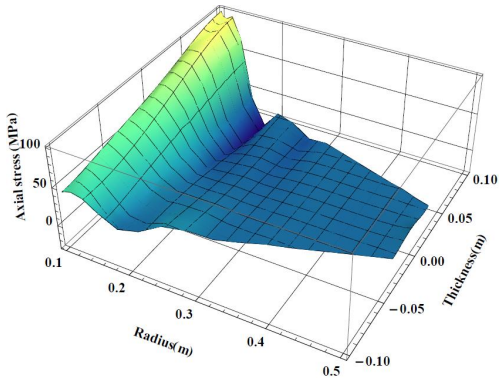


(c) Axial stress at the linear shape

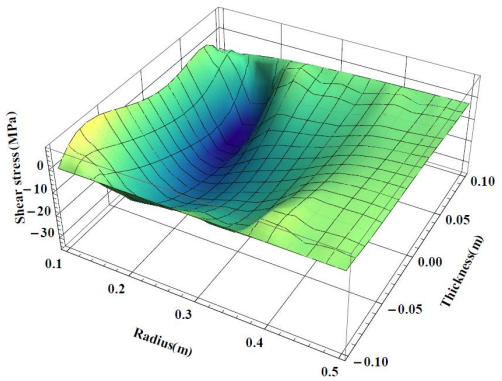


(d) Shear stress at the constant shape

Figure 15: 3-D Stress distribution with $n_r = 2$, $n_z = 3$.

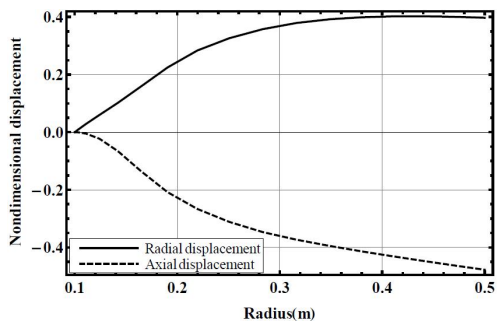


(a) Non-dimensional displacement via the radius

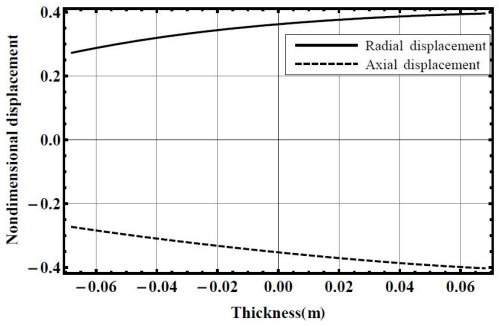


(b) Non-dimensional displacement via the thickness

Figure 16: Non-dimensional displacement at the middle thickness via radial direction and at the middle radius via axial direction.

the power exponents law and changes significantly with increasing $n_r$.

Fig. 20 presents the non-dimensional radial and axial displacement along the thick-

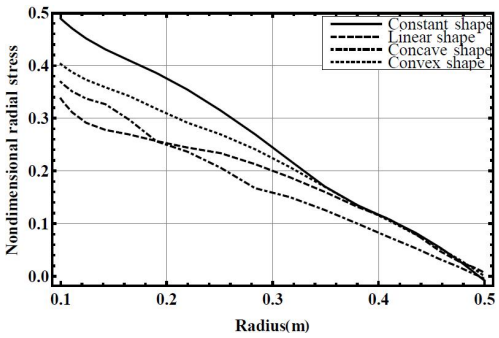


(a) Non-dimensional radial stress via the radius

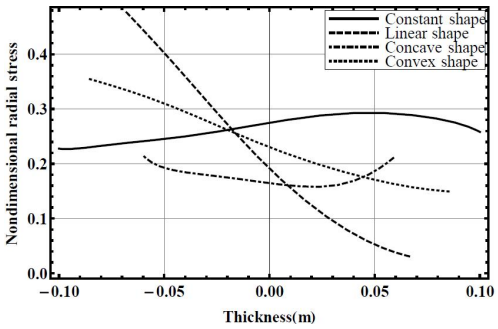


(b) Non-dimensional radial stress via the thickness

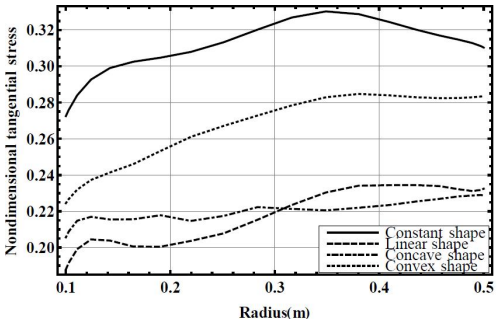


(c) Non-dimensional tangential stress via the radius

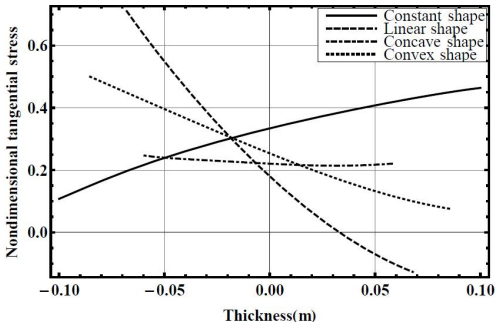


(d) Non-dimensional tangential stress via the thickness

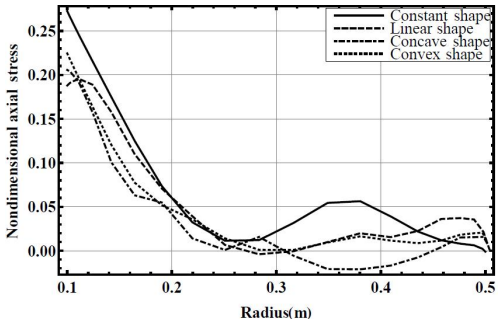


(e) Non-dimensional axial stress via the radius

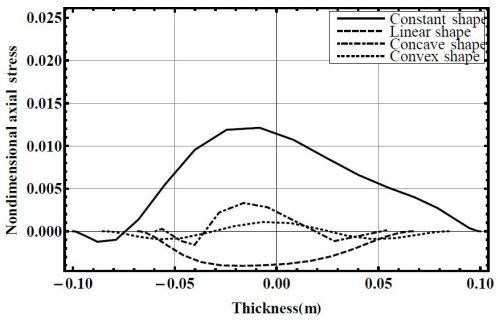


(f) Non-dimensional axial stress via the thickness

Figure 17: Non-dimensional stresses distribution in various profile shapes with $n_r = 1.5$, $n_z = 3$.

ness at $r = 0.33b$ in a constant thickness profile shape. As can be seen with an increase of $n_r$ and decrease of $n_z$ the non-dimensional displacements rise.

## 6 Conclusions

In this paper a thick FG rotating disk with two dimensional pattern of heterogeneity is analyzed using two dimensional generalized differential quadrature method which is

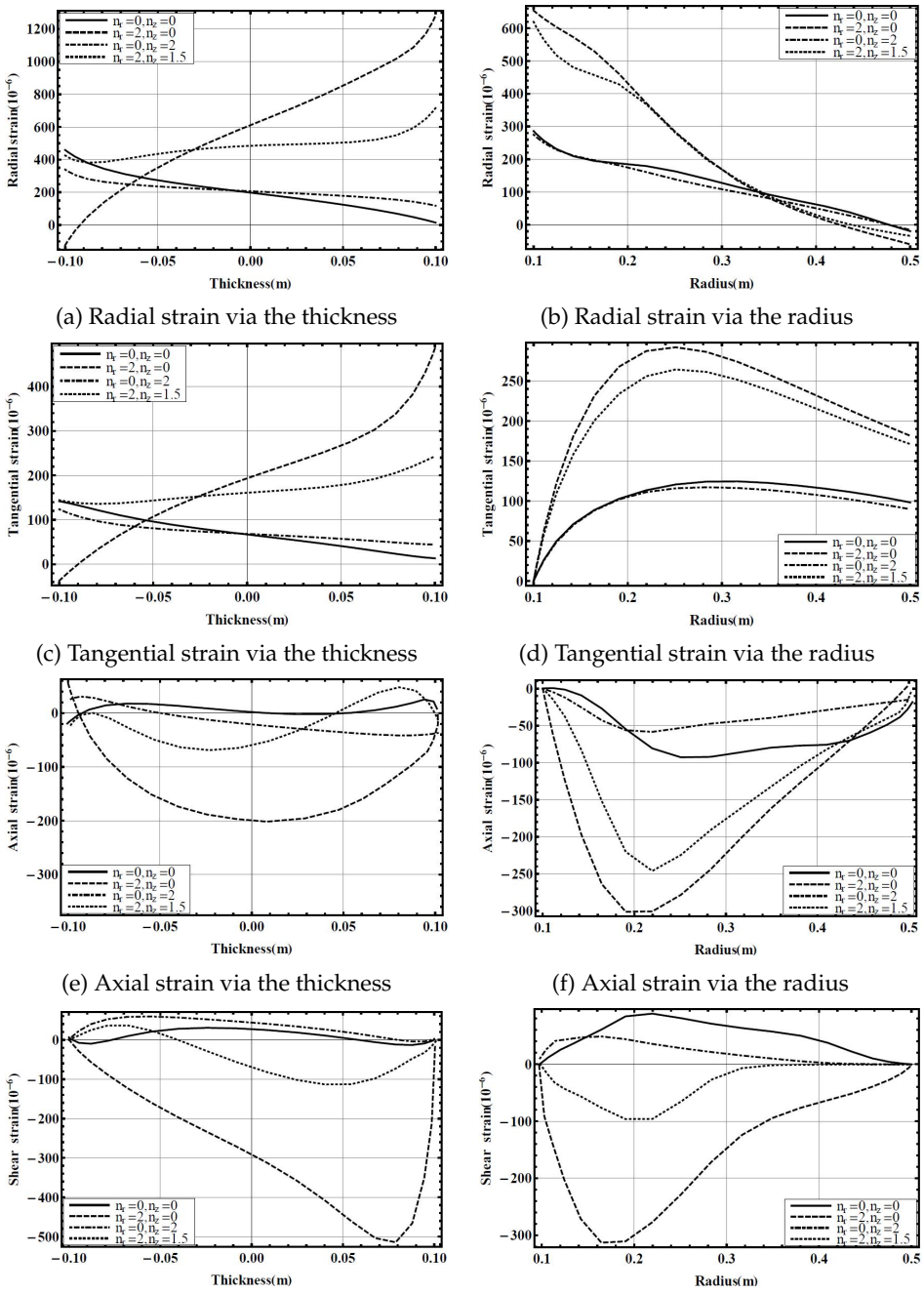


(a) Radial strain via the thickness

(b) Radial strain via the radius

(c) Tangential strain via the thickness

(d) Tangential strain via the radius

(e) Axial strain via the thickness

(f) Axial strain via the radius

(g) Shear strain via the thickness

(h) Shear strain via the radius

Figure 18: Strain distribution in constant profile shapes with different combinations of power exponent.

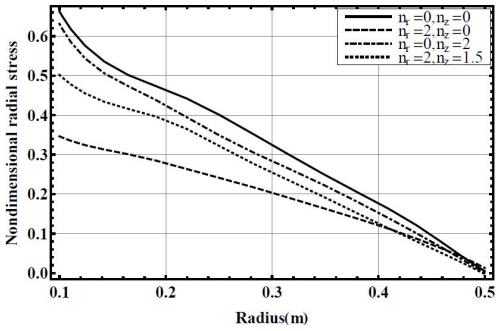


(a) Non-dimensional radial stress via the radius

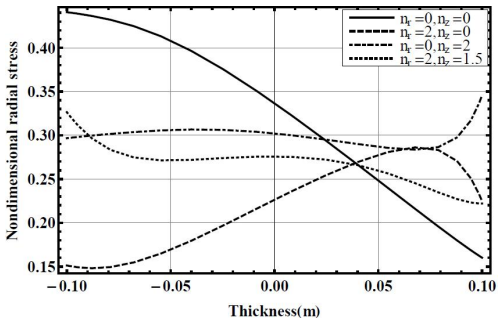


(b) Non-dimensional radial stress via the thickness

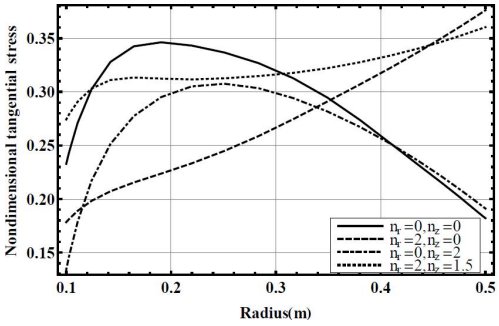


(c) Non-dimensional tangential stress via the radius

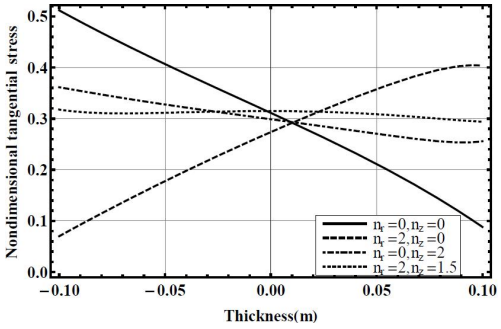


(d) Non-dimensional tangential stress via the thickness

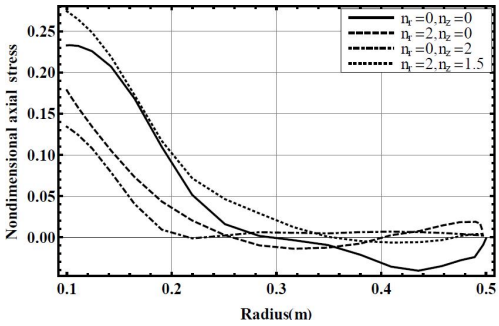


(e) Non-dimensional axial stress via the radius

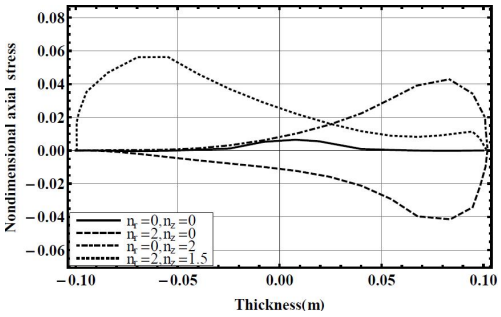


(f) Non-dimensional axial stress via the thickness

Figure 19: Non-dimensional stress distribution in constant profile shapes with different combinations of power exponent.

applied in a non-uniform geometrical model of disks. Four different profile shapes of the disk are considered all of them fixed at inner radius and have traction free condition in the other surfaces boundaries. Furthermore four different combination types of power exponents are used and the effects of particle distribution pattern on the response of the disk are discussed. Results show that the disk with constant shape is not a suitable choice for selecting a thick FG disk, it means in order to reach better conditions of stresses and strains the non-uniform profile shape is an inevitable model. Among four different pro-

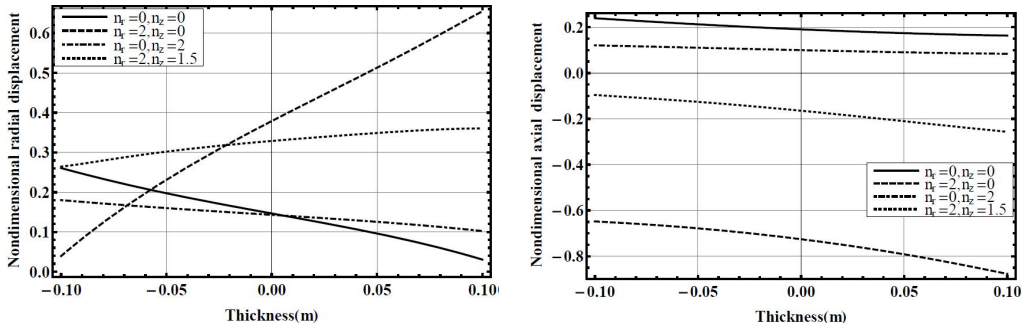


Figure 20: Non-dimensional radial and axial distribution along the thickness in constant profile shapes with different combinations of power exponent.

file types, the parabolic concave profile has a better response than all and can be efficient for applied design. In about the power distribution of materials it can be said that the isotropic disk and also the disk with the only radial distribution of particle contents have a serious condition and it must to reinforced the disk along the axial direction it means that consideration of material inhomogeneity in two directions leads to a more flexible design and also exact analysis of thick FG rotating disks. Therefore the best composition of power exponent consists of the lower value of $n_r$ and larger value of $n_z$, herein using the two dimensional functionally graded materials leads to an accurate design. Results comparison with the other published literature show a good agreement, however the time spent by different methods for solving the same problem is much higher.

# Appendix

$$\lambda_1=\frac{E(1-v)}{1-v-2v^2},\quad \lambda_2=G,\quad \lambda_3=\frac{Ev}{1-v-2v^2}+G,$$
$$\lambda_4=\frac{1-v}{1-v-2v^2}\frac{\partial E}{\partial r}+\frac{2vE(2-v)}{(1-v-2v^2)^2}\frac{\partial v}{\partial r}+\frac{E(1-v)}{r(1-v-2v^2)},$$
$$\lambda_5=\frac{v}{1-v-2v^2}\frac{\partial E}{\partial r}+\frac{E\left(1+2v^2\right)}{(1-v-2v^2)^2}\frac{\partial v}{\partial r}+\frac{\partial G}{\partial z},\quad \lambda_6=\frac{\partial G}{\partial z},$$
$$\lambda_7=\frac{v}{1-v-2v^2}\frac{\partial E}{\partial r}+\frac{E\left(1+2v^2\right)}{(1-v-2v^2)^2}\frac{\partial v}{\partial r}+\frac{E(v-1)}{r(1-v-2v^2)},\quad \lambda_8=\frac{-1}{1-2v}\frac{\partial E}{\partial r}-\frac{2E}{(1-2v)^2}\frac{\partial v}{\partial r},$$
$$\lambda_9=\frac{-E(1+v)}{1-v-2v^2},\quad \lambda_{10}=\frac{v-1}{1-v-2v^2}\frac{\partial E}{\partial r}+\frac{2vE(v-2)}{(1-v-2v^2)^2}\frac{\partial v}{\partial r}+\frac{E(2v-1)}{r(1-v-2v^2)},$$
$$\beta_1=\frac{E(1-v)}{1-v-2v^2},\quad \beta_2=G,\quad \beta_3=\frac{Ev}{1-v-2v^2}+G,$$

$$\beta_4=\frac{v}{1-v-2v^2}\frac{\partial E}{\partial z}+\frac{E\left(1+2v^2\right)}{\left(1-v-2v^2\right)^2}\frac{\partial v}{\partial z},\quad \beta_5=\frac{Ev}{r(1-v-2v^2)}\frac{\partial G}{\partial r}+\frac{G}{r},$$
$$\beta_6=\frac{v}{1-v-2v^2}\frac{\partial E}{\partial z}+\frac{E\left(1+2v^2\right)}{\left(1-v-2v^2\right)^2}\frac{\partial v}{\partial z},\quad \beta_7=\frac{\partial G}{\partial r}+\frac{G}{r},$$
$$\beta_8=\frac{1-v}{1-v-2v^2}\frac{\partial E}{\partial z}+\frac{2Ev(2-v)}{\left(1-v-2v^2\right)^2}\frac{\partial v}{\partial z},\quad \beta_9=\frac{-1}{1-2v}\frac{\partial E}{\partial z}+\frac{2E}{(1-2v)^2}\frac{\partial v}{\partial z},\quad \beta_{10}=\frac{-E(1+v)}{1-v-2v^2}.$$

## Acknowledgements

Author gratefully acknowledge Dr. Nicholas Fantuzzi for the time spent on this occasion. I received very instructive and useful comments that enhanced the content of the paper.

## References

[1] A. K. Thawait, L. Sondhi, Sh. Sanyal, and Sh. Bhowmick, *Elastic analysis of functionally graded variable thickness rotating disk by element based material grading,* J. Solid Mech., 9(3)(2017), pp. 650–662.

[2] A. M. Afsar, and J. Go, *Finite element analysis of thermoelastic field in rotating FGM circular disk,* Appl. Math. Model., 34(11) (2010), pp. 3309–3320.

[3] M. Asghari, and E. Ghafoori, *A three-dimensional elasticity solution for functionally graded rotating disks,* Compos. Struct., 92(5) (2010), pp. 1092–1099.

[4] V. Vullo, and F. Vivio, *Elastic stress analysis of non-linear variable thickness rotating disks subjected to thermal load and having variable density along the radius,* Int. J. Solids Struct., 45(20) (2008), pp. 5337–5355.

[5] G. J. Nie, and R. C. Batra, *Stress analysis and material tailoring in isotropic linear thermoelastic incompressible functionally graded rotating disks of variable thickness,* Compos. Struct., 92(3) (2010), pp. 720–729.

[6] H. Jahed, B. Farshi, and J. Bidabadi, *Minimum weight design of inhomogeneous rotating discs,* Int. J. Pressure Vessels Piping, 82(1) (2005), pp. 35–41.

[7] N. N. Alexandrova, S. Alexandrov, and P. M. M. Vila Real, *Analysis of stress and strain in a rotating disk mounted on a rigid shaft,* J. Theor. Appl. Mech., 33(1) (2006), pp. 65–90.

[8] M. Hosseini, M. Shishesaz, Kh. Naderan Tahan, and A. Hadi, *Stress analysis of rotating nano-disks of variable thickness made of functionally graded materials,* Int. J. Eng. Sci., 109 (2016), pp. 29–53.

[9] B. Farshi, H. Jahed, and A. Mehrabian, *Optimum design of inhomogeneous non-uniform rotating discs,* Comput. Struct., 82(9-10) (2004), pp. 773–779.

[10] K. Mercan, C. Demir and O. Civalek, *Vibration analysis of FG cylindrical shells with power-law index using discrete singular convolution technique,* Curved and Layer Structures, 3(1) (2016), pp. 82–90.

[11] C. Shu, and C. M. Wang, *Treatment of mixed and nonuniform boundary conditions in GDQ vibration analysis of rectangular plates,* Eng. Struct., 21(2) (1999), pp. 125–134.

[12] O. CIVALEK, *Free vibration analysis of symmetrically laminated composite plates with first order shear deformation theory (FSDT) by discrete singular convolution method,* Finite Elements in Analysis and Design, 44 (2008), pp. 725–731.

[13] H. ZAFARMAND, AND M. KADKHODAYAN, *Nonlinear analysis of functionally graded nanocomposite rotating thick disks with variable thickness reinforced with carbon nanotubes,* Aerospace Science and Technology, 41 (2015), pp. 47–54.

[14] Y. ZHENG, H. BAHALOO, D. MOUSANEZHAD, E. MAHDI, A. VAZIRI, AND H. NAYEB HASHEMI, *Stress analysis in functionally graded rotating disks with non-uniform thickness and variable angular velocity,* Int. Mech. Sci., 119 (2016), pp. 283–293.

[15] M. BAYAT, M. SALEEM, B. B. SAHARI, A. M. S. HAMOUDA, AND E. MAHDI, *Analysis of functionally graded rotating disks with variable thickness,* Mech. Res. Commun., 35(5) (2008), pp. 283–309.

[16] M. N. M. ALLAM, R. TANTAWY, AND A. M. ZENKOUR, *Thermoelastic stresses in functionally graded rotating annular disks with variable thickness,* J. Theor. Appl. Mech., 56(4) (2018), pp. 1029–1041.

[17] J. SLADEK, V. SLADEK, AND CH. ZHANG, *Stress analysis in anisotropic functionally graded materials by the MLPG method,* Eng. Anal. Boundary Elements, 29(5) (2005), pp. 597–609.

[18] A. HASSANI, M. H. HOJJATI, G. H. FARRAHI, AND R. A. ALASHTI, *Semi-exact solution for thermo-mechanical analysis of functionally graded elastic-strain hardening rotating disks,* Commun. Nonlinear Sci. Numer. Simul., 17(9) (2012), pp. 3747–3762.

[19] H. ZHARFI, AND H. EKHTERAEI TOUSSI, *Numerical creep analysis of FGM rotating disc with GDQ method,* J. Theor. Appl. Mech., 55(1) (2017), pp. 331–341.

[20] H. ZHARFI, AND H. EKHTERAEI TOUSSI, *Time dependent creep analysis in thick FGM rotating disk with two-dimensional pattern of heterogeneity,* Int. J. Mech. Sci., 140 (2018), pp. 351–360.

[21] R. BELLMAN, B. G. KASHEF, AND J. CASTI, *Differential quadrature: a technique for the rapid solution of nonlinear partial differential equations,* J. Comput. Phys., 10(1) (1972), pp. 40–52.

[22] C. SHU, AND B. E. RICHARDS, *Application of generalized differential quadrature to solve two-dimensional incompressible Navier-Stokes equation,* Int. J. Numer. Methods Fluids, 15(7) (1992), pp. 791–798.

[23] O. CIVALEK, AND M. ULKER, *Harmonic differential quadrature (HDQ) for axisymmetric bending analysis of thin isotropic circular plates,* Struct. Eng. Mech., 17(1) (2004), pp. 1–14.

[24] F. TORNABENE, N. FANTUZZI, AND M. BACCIOCCHI, *The GDQ method for the free vibration analysis of arbitrarily shaped laminated composite shells using a NURBS-based isogeometric approach,* Compos. Struct., 154(1) (2016), pp. 190–218.

[25] F. TORNABENE, A. LIVERANI, AND G. CALIGIANA, *Laminated composite rectangular and annular plates: a GDQ solution for static analysis with a posteriori shear and normal stress recovery,* Compos. Part B, 43(4) (2012), pp. 1847–1872.

[26] H. ZHARFI, AND H. EKHTERAEI TOUSSI, *Non-steady creep analysis of FGM rotating disc using GDQ method,* Adv. Appl. Math. Mech., 11(1) (2019), pp. 1–15.

[27] A. FEREIDOON, A. M. BABAEE, AND Y. ROSTAMIYAN, *Application of generalized differential quadratre method to nonlinear bending analysis of a single SWCNT over a bundle of nanotubes,* Arch. Mech., 64(4) (2012), pp. 347–366.

[28] F. TORNABENE, AND A. CERUTI, *Free-form laminated doubly-curved shells and panels of revolution resting on Winkler–Pasternak elastic foundations: a 2-D GDQ solution for static and free vibration analysis,* World J. Mech., 3(1) (2013), pp. 1–25.

[29] P. A. A. LAURA, AND R. H. GUTIERREZ, *Analysis of vibration rectangular plates with non-uniform boundary conditions by using the differential quadrature method,* J. Sound Vib., 173(5)

(1994), pp. 702–706.

[30] C. W. BERT, S. K. JANG, AND A. G. STRIZ, *Two new approximate methods for analyzing free vibration of structural components,* AIAA J., 26(5) (1988), pp. 612–618.

[31] S. K. JANG, C. W. BERT, AND A. G. STRIZ, *Application of differential quadrature to static analysis of structural components,* Int. J. Numer. Methods Eng., 28(3) (1989), pp. 561–577.

[32] C. SHU, AND H. DU, *Implementation of clamped and simply supported boundary conditions in the GDQ free vibration analysis of beams and plates,* Int. J. Solids Struct., 34(7) (1997), pp. 819–835.

[33] H. ZAFARMAND, AND B. HASSANI, *Analysis of two-dimensional functionally graded rotating thick disks with variable thickness,* Acta Mech., 225(2) (2014), pp. 453–464.

[34] B. KIEBACK, A. NEUBRAND, AND H. RIEDEL, *Processing techniques for functionally graded materials,* Mater. Sci. Eng. A, 362(1-2) (2003), pp. 81–106.